JOURNAL OF GEOPHYSICAL RESEARCH, VOL. 104, NO. A5, PAGES 10,317–10,326, MAY 1, 1999

Free energy sources and frequency bandwidth for the auroral kilometric radiation

P. L. Pritchett

Department of Physics and Astronomy, University of California, Los Angeles

R. J. Strangeway

Institute of Geophysics and Planetary Physics, University of California, Los Angeles

C. W. Carlson, R. E. Ergun, J. P. McFadden, and G. T. Delory

Space Sciences Laboratory, University of California, Berkeley

Abstract. Electron distributions obtained in the source regions of auroral kilometric radiation (AKR) by the Fast Auroral SnapshoT (FAST) satellite have revealed several free energy sources with positive gradients with respect to $v_\perp$ superimposed on a broad plateau with a radius close to the primary incident electron acceleration energy and covering pitch angles from near field-aligned all the way to the (upgoing) loss cone. Two-dimensional electromagnetic particle simulations are used to demonstrate that such a distribution arises as a quasi-steady feature of a process in which the increase of the perpendicular velocity of the electrons as they propagate into a region of increasing magnetic field strength is balanced by the diffusion to lower $v_\perp$ caused by the electron-cyclotron maser instability. The maser radiation is emitted nearly perpendicular to the ambient magnetic field at frequencies between the relativistic and nonrelativistic cyclotron frequencies. In these circumstances, the entire primary auroral electron distribution can contribute to the resonant wave-particle interaction, leading to electric field intensities of the order of 500 mV/m. In contrast, a pure loss cone distribution is shown to produce much weaker electric fields, leads to emission at angles $\gtrsim 10°$ away from perpendicular, and cannot produce the broad plateau observed in the electron distribution. The simulations and linear theory indicate that the maser instability in a uniform system produces an intrinsic bandwidth of the order of a few tenths of 1% of the cyclotron frequency (~0.5–1.0 kHz in the AKR source region). Any narrower spectra would appear to require some nonuniform or time-dependent feature in the source region.

1. Introduction

The auroral kilometric radiation (AKR) was originally discovered as electromagnetic radiation propagating away from the Earth [*Benediktov et al.*, 1965]. Subsequent work clearly established that AKR is generated at high altitudes over the auroral regions in association with bright auroral arcs [*Gurnett*, 1974; *Kurth et al.*, 1975]. AKR is the dominant plasma emission in the auroral zone at frequencies greater than 1 kHz [*Gurnett et al.*, 1983]; the typical power radiated is of the order of 10^7 W, while the peak power level can be as large as 10^9 W.

Paper number 1998JA900179.
0148-0227/99/1998JA900179$09.00

It is now generally agreed that the most likely mechanism for the generation of AKR (as well as its analogs at Jupiter, Saturn, and Uranus) is the electron-cyclotron maser instability [*Wu and Lee*, 1979]. The cyclotron maser mechanism provides the following characteristic predictions: (1) emission occurs near the local electron cyclotron frequency Ω_e; (2) the plasma frequency ω_{pe} in the source region must be much smaller than Ω_e; (3) generation of the radiation occurs primarily in the right-hand extraordinary (R-X) mode. There is now strong evidence supporting all of these features. Despite these successes of the maser instability in explaining the general features of AKR, there remain several fundamental unanswered questions regarding the generation process. Two of the most significant are the identification of the precise free-energy source that drives the maser instability and the explanation of the fine structure appearing at frequencies of 1 kHz and lower.

There are at least three possibilities for the free-energy source. (1) The source originally suggested by *Wu and Lee* [1979] was the loss cone associated with the upgoing electrons that have mirrored in the geomagnetic field. That this feature is the dominant source has been questioned on the basis of two-dimensional (2-D) particle simulations employing a model auroral zone electron distribution function [*Pritchett and Strangeway*, 1985] and Viking observations [*Ungstrup et al.*, 1990; *Louarn et al.*, 1990; *Roux et al.*, 1993]. The latter revealed that at the edge of the AKR source region (as opposed to the interior) there is frequently a well-pronounced loss cone, and yet AKR is not generated there. It thus appears that the presence of a loss cone is not sufficient for AKR generation [*Louarn et al.*, 1990]. (2) The upward directed parallel electric field in the auroral acceleration region should tend to accelerate plasma sheet electrons downward to form a beam-like distribution. As these electrons move down the field lines into an increasing magnetic field, their pitch angle should increase due to conservation of the first adiabatic invariant. The electron distribution should thus have a peak at large pitch angles and a hole at small pitch angles [*Winglee and Pritchett*, 1986]. This produces a large region of the distribution function with $\partial f/\partial v_\perp > 0$ and leads to emission nearly perpendicular to the magnetic field. (3) In the presence of a constant electric field, there is a region of velocity space which is inaccessible (in the absence of collisions or diffusion) to electrons of either magnetospheric or ionospheric origin [*Chiu and Schulz*, 1978]. Nevertheless, the Viking observations indicate that this region is not depleted; rather, it shows a broad plateau and sometimes even a positive slope [*Louarn et al.*, 1990]. It has been suggested that this region of trapped electrons is formed when the electrons experience a time-varying electric field and that it is the trapped electrons around $v_\parallel \approx 0$ that produce the positive $\partial f/\partial v_\perp$ gradient and thus drive the maser instability.

A characteristic feature of AKR is the fine structure [*Gurnett et al.*, 1979]. In high resolution spectra AKR is observed to consist of many closely spaced, narrowband (~1 kHz) components that display a high degree of variability with time, sometimes rising, sometimes falling, and sometimes showing quite convoluted behavior [*Gurnett and Anderson*, 1981]. Furthermore, the bandwidth of these tones is quite variable, with values as low as 5 Hz having been inferred [*Baumback and Calvert*, 1987]. One possible explanation for such extremely narrow spectral features is the feedback mechanism leading to radio lasing [*Calvert*, 1982, 1995]. In addition, it has been stressed by *Le Quéau et al.* [1985] that the inhomogeneity of the magnetic field should play a crucial role in determining the AKR spectrum.

The Fast Auroral SnapshoT (FAST) satellite has made wave and 3-D electron observations in the AKR source region with unprecedented frequency and time resolution [*Ergun et al.*, 1998; *Delory et al.*, 1998]. The AKR emissions were observed to have strong temporal and/or spatial variations. Of particular significance was the observation of peak electric field amplitudes in the source region typically greater than 100 mV/m and reaching as high as 300 mV/m (the saturation level of the FAST instrument at AKR frequencies). These large amplitudes were seen in short bursts of ~100-ms duration. These peak amplitudes are considerably larger than the level of 20–50 mV/m reported by Viking [*de Feraudy et al.*, 1987] in the source region. Since the Viking results were obtained with a swept frequency analyzer with a sweeping time of 2.4 s, the sweeper may have missed the very short duration bursts. The electron data display a broad plateau over a wide range of pitch angles, indicating that the distributions have been rapidly stabilized by AKR wave growth. The FAST observations confirm that the AKR source is in a density-depleted cavity that is dominated by hot electrons and is nearly void of low-energy electrons [*Strangeway et al.*, 1998a]. The source region emissions are typically within ~2% of Ω_e and occasionally fall below Ω_e, which is consistent with the strong modification of the plasma dispersion from the cold wave approximation predicted for density-depleted cavities satisfying $\omega_{pe}/\Omega_e < v_{Te}/c$ [*Pritchett*, 1984; *Pritchett and Strangeway*, 1985; *Strangeway*, 1985; *Winglee and Pritchett*, 1986].

In the present work we use the detailed FAST electron distributions to examine the questions of free-energy source and inherent bandwidth for the cyclotron maser mechanism. This is done by constructing electron particle distributions which are used as input to 2-D, initial value, relativistic, electromagnetic particle simulations. The particle distributions are qualitatively similar to those used previously by *Pritchett and Strangeway* [1985] and *Winglee and Pritchett* [1986], but now the simulations have much higher grid resolution and number of particles so that the condition $\Omega_e/\omega_{pe} \gtrsim 50$ characteristic of the AKR source region can be adequately modeled. The results of the simulations show that the very intense fields observed by FAST can be produced by the maser instability if the entire primary auroral electron distribution can contribute to the resonant wave-particle interaction. In contrast, a purely upgoing loss cone produces much weaker emissions. The characteristic bandwidth observed in the simulations for the case of a uniform system with no feedback mechanism is found to be $\Delta\omega/\Omega_e \sim 2\text{–}3 \times 10^{-3}$, where $\Delta\omega$ is the full width at the $1/e$ power points. These results are confirmed by linear theory calculations and estimates for the observed number of e-foldings required to produce the observed AKR power levels. For the value $\Omega_e/2\pi \approx 440$ kHz typical of the FAST observations, this yields a frequency bandwidth of ~1 kHz. This is considerably larger than most of the fine structure observed by FAST.

The outline of the paper is as follows. In section 2 we discuss the FAST particle measurements and con-

struct an electron distribution function $f(v_\parallel, v_\perp)$ that is suitable for use in an initial value simulation. Section 3 presents the results of particle simulations using this FAST-based $f(v_\parallel, v_\perp)$ as well as an upgoing loss cone. Section 4 discusses the frequency bandwidth of the electron-cyclotron maser instability based on linear theory applied to a simple model distribution function. Section 5 contains the summary and discussion.

2. Electron Distribution Function

Plate 1 shows electron contour plots in $v_\parallel$,$v_\perp$ space from a FAST crossing of the AKR source region on orbit 1761. The crossing occurred near 22 MLT, and the electron data were averaged over a 40 s interval near 06:44 UT. Figure 1 of *Strangeway et al.* [1998a] shows additional particle and field data from the same pass during the interval 06:42–06:47 UT. During the central part of this longer interval, there are intense wave emissions extending down to, and even slightly below, the local electron-cyclotron frequency f_{ce}. In addition, the electron and ion spectra are relatively monoenergetic, with an absence of low-energy electrons and with the ions narrowly confined to a few degrees around 180° pitch angle (corresponding to upgoing particles). These features indicate that the accelerating electric field structure extends both above and below the FAST spacecraft. The most notable features of the velocity space plot in Plate 1 are the presence of a clear beam structure at $v_\perp = 0$ and $v_\parallel \sim 2.7 \times 10^4$ km/s and a broad enhancement extending in a nearly circular arc from the beam feature all the way into the upgoing part of the distribution. Near 90° pitch angles, there is a broad plateau in the distribution, and on the upgoing side, there is a clear loss cone feature.

The features of the distribution in Plate 1 are quite similar to those expected for a beam of primary auroral electrons accelerated by a parallel electric field and propagating into a region of increasing magnetic field strength [*Winglee and Pritchett*, 1986], and they show a striking resemblance to the results of particle simulations obtained for the case of an auroral distribution with the hot electron population exceeding the cold electron population, $n_{\rm hot} > n_{\rm cold}$ (see Figure 15b of *Winglee and Pritchett* [1986].)

It is known from theoretical considerations [*Le Quéau et al.*, 1984b] and confirmed by the particle simulations [e.g., *Pritchett*, 1986a] that the diffusion produced by the resonant interaction of strongly supraluminous waves ($\omega/k_\parallel c \gg 1$) with weakly relativistic electrons occurs almost entirely in $v_\perp$, with $v_\parallel$ remaining constant. This diffusion leads to a reduction in the $\partial f/\partial v_\perp$ gradient that drives the instability, and saturation of the maser instability appears to occur as a result of quasi-linear diffusion [*Wu et al.*, 1981a; *Pritchett*, 1986a]. Thus the broad plateau observed in Plate 1 and in the additional distributions discussed by *Delory et al.* [1998] is consistent with a process in which the primarily monoenergetic auroral electron distribution has been spread to large pitch angles by propagating into the increasing geomagnetic field and diffused to smaller values of $v_\perp$ by the maser instability.

In order to determine an electron distribution that is suitable for use in an initial value particle simulation, one should remove the effects of this diffusion in $v_\perp$. Thus we have integrated the FAST distribution shown in Plate 1 over $v_\perp$ to obtain a reduced distribution $\tilde{f}(v_\parallel)$,

$$\tilde{f}(v_\parallel) = \int_{E>400\text{eV}} 2\pi v_\perp f(v_\parallel, v_\perp) dv_\perp. \qquad (1)$$

The integration is restricted to energies above 400 eV to avoid contamination from photoelectrons. The distribution $\tilde{f}$ is then centered along the elliptical arc representing the accessibility boundary for electrons of magnetospheric origin [*Chiu and Schulz*, 1978; *Pritchett and Strangeway*, 1985], terminated at an upgoing pitch angle of 45°, and given a velocity spread of $\Delta v/c \approx 0.007$. The resulting distribution in $v_\parallel$,$v_\perp$ space is shown in Figure 1. We shall adopt the descriptive name "horseshoe" to refer to this type of distribution. (A similar feature was observed in DE 1 electron distributions by *Menietti et al.* [1993], which they referred to as a "banana" distribution.)

3. Simulation Results

We now perform 2-D, initial value, electromagnetic particle simulations using the distribution shown in Figure 1. For comparison we will also show the results obtained using a purely thermal particle population with a perfectly sharp loss cone boundary at an upgoing angle of 45°. The 2-D particle code is similar to that used previously by *Pritchett and Strangeway* [1985] and *Winglee and Pritchett* [1986], except that it is now possible to use a much larger number of grid points and particles. The results discussed in this section employ an $L_x \times L_y = 512\Delta \times 128\Delta$ grid (with the external magnetic field oriented parallel to the y axis) and 1,440,000 particles. The grid spacing Δ is $\approx$0.12 km. The exter-

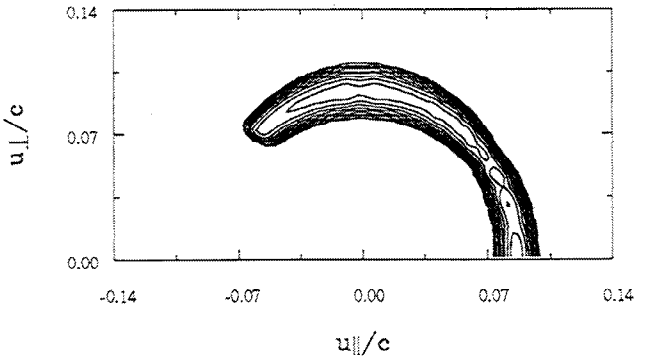

Figure 1. The initial electron distribution function $f(u_\parallel, u_\perp)$ used in the particle simulations. The value of f changes by a factor of 2 between adjacent contours.

nal magnetic field and plasma density are assumed to be spatially uniform, periodic boundary conditions are assumed in both the x and y directions, and the ions are kept fixed during the simulation. The time step is taken to be $\Omega_e \Delta t = 0.2$. Once the initial electron distribution is specified, the only remaining parameter in the simulation is Ω_e/ω_{pe}. For a typical density of 0.6 cm^{-3} and a cyclotron frequency of 400 kHz, this ratio is 57. We shall use the value $\Omega_e/\omega_{pe} = 50$ in the simulations.

Figure 2 shows the time history of the total electromagnetic energy (normalized to the initial electron kinetic energy) produced by the horseshoe distribution of Figure 1. As expected, there is a strong maser instability excited by this distribution. The linear growth rate for the fastest growing mode is $\gamma/\Omega_e = 3.1 \times 10^{-3}$. The instability saturates at $\Omega_e t \approx 2800$. At this time the peak electric field is approximately 500 mV/m. This is comparable to or slightly larger than the peak fields observed by FAST [*Ergun et al.*, 1998]. It is thus clear that the horseshoe type distribution has enough free energy to produce the most intense observed levels of AKR. In contrast, the simulation using a perfectly sharp upgoing loss cone distribution produces a much weaker maser instability. As shown in Figure 2, the growth rate is much smaller, $\gamma/\Omega_e \sim 9 \times 10^{-4}$, and the maximum radiation energy produced is smaller by a factor of 12. It thus seems to be very likely that the most intense AKR must be produced by a process involving the entire primary auroral electron distribution.

Figure 3 shows the development of the electron distribution function in the simulation using the horseshoe distribution. Figure 3a shows the initial distribution, while Figure 3b shows the distribution at saturation. It is clear that diffusion to smaller values of $v_\perp$ has almost

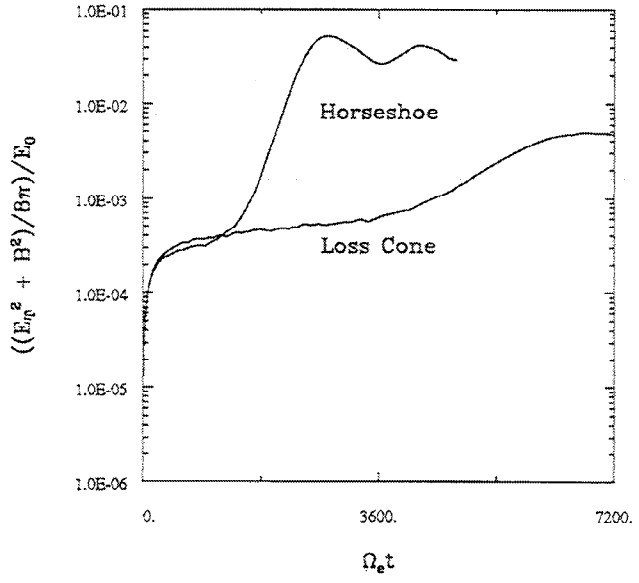

Figure 2. Time history of the total electromagnetic energy (normalized to the initial electron kinetic energy E_0) produced in 2-D particle simulations using a horseshoe distribution and a 45° upgoing loss cone.

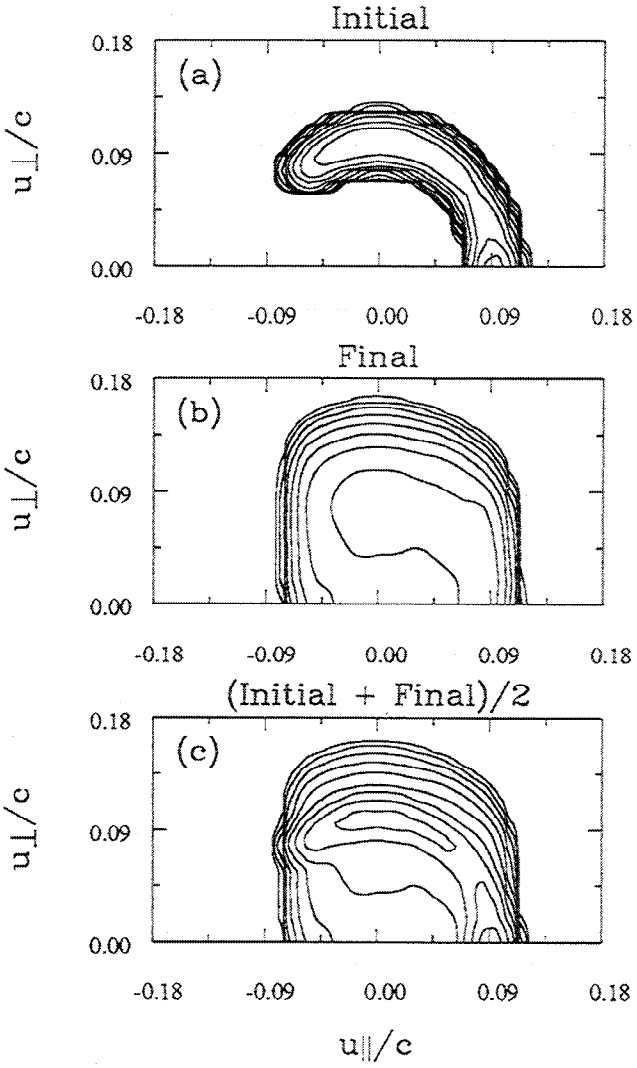

Figure 3. Contours of the electron distribution $f(u_\parallel, u_\perp)$ in the 2-D simulation using a horseshoe distribution. (a) Initial distribution, (b) distribution at saturation ($\Omega_e t = 4800$), (c) average of the distributions in a and b. The value of f changes by a factor of 2 between adjacent contours.

completely eliminated the positive $\partial f/\partial v_\perp$ slope in the initial distribution. (There is also some migration to larger values of $v_\perp$. This occurs due to scattering of the electrons to higher $v_\perp$ by the radiation which is retained in the system due to the assumption of periodic boundary conditions. This effect would be significantly reduced in an open system where the radiation is allowed to escape from the source region [*Pritchett*, 1986b].) In addition, the beam feature at $v_\perp \approx 0$ has been removed. Figure 3c shows the average of the initial and saturation distributions. This average exhibits qualitatively many of the features in the original FAST distribution of Plate 1 including the beam feature, enhancement along the elliptical accessibility boundary for magnetospheric electrons, and a (weak) loss cone. This panel supports the interpretation that the FAST observations represent a quasi-steady condition in which the introduction of new

magnetospheric electrons is balanced against the diffusion to smaller values of $v_\perp$ caused by the maser instability. In contrast, Figure 4 shows the initial and final electron distribution functions in the simulation using the upgoing loss cone. Here the diffusion is confined to the upgoing side, and the downgoing electrons are basically unaffected by the development of the maser instability. Thus a loss cone driven maser instability could not explain the observed plateau in the downgoing electron distribution.

Figure 5 shows the power spectrum for the E_z electric field averaged over the entire duration $0 \le \Omega_e t \le 4800$ of the simulation. The peak frequency occurs at $\omega/\Omega_e = 0.994$, and the full width at half maximum is $\Delta\omega/\Omega_e \approx 0.003$. Figure 6 shows a similar plot for the simulation with the 45° loss cone; here the duration of the run is $0 \le \Omega_e t \le 7200$. Now the dominant mode has a finite value of $k_\parallel$ ($k_\parallel/k_\perp \approx 0.21$) which Doppler shifts the observed frequency of $\omega/\Omega_e = 1.007$ down to the gyrofrequency. The bandwidth is about the same as before. This substantial value of $k_\parallel$ corresponds to wave propagation at an angle of ≈12° away from perpendicular to the magnetic field. In contrast, the FAST observations within the source region [*Ergun et al.*, 1998] reveal that the emission is within 3° of perpendicular and is consistent with $k_\parallel = 0$.

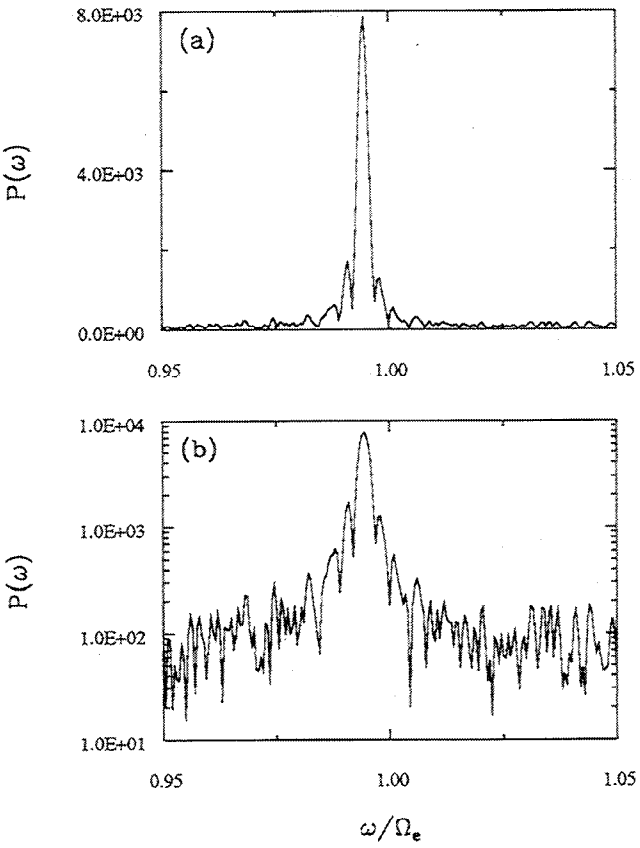

Figure 5. Power spectrum in the frequency range $0.95 \le \omega/\Omega_e \le 1.05$ computed over the entire duration of the simulation using the horseshoe distribution: (top) linear scale; (bottom) logarithmic scale.

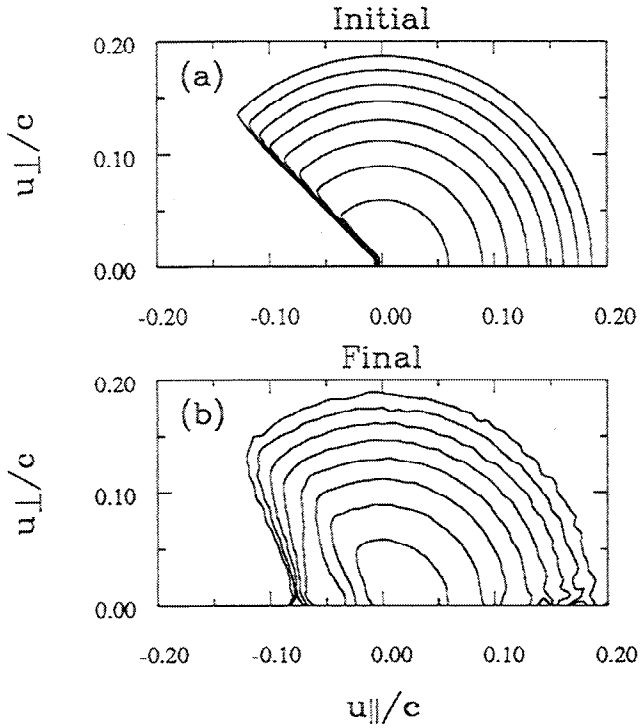

Figure 4. Contours of the electron distribution $f(u_\parallel, u_\perp)$ in the 2-D simulation using a 45° upgoing loss cone distribution. (a) Initial distribution, (b) final distribution ($\Omega_e t = 7200$). The value of f changes by a factor of 2 between adjacent contours.

4. Bandwidth of the Maser Instability

The power spectra in Figures 5 and 6 represent the effect of the evolution of the maser instability over a number of e-foldings. In this section we use the results of a linear theory calculation of the maser instability bandwidth to estimate how the power spectrum should sharpen as a function of the number of e-foldings. We compare these estimates with the simulation results and the FAST observations.

In evaluating the dispersion relation for the linearized Vlasov-Maxwell equations for the conditions of the AKR source region, it is essential to solve the full relativistic dispersion relation [*Pritchett and Strangeway*, 1985]. Any attempt at an approximate calculation which is based on retaining the results of cold plasma theory for the wave dispersion introduces significant errors in the growth rates and angular distributions [*Pritchett*, 1986a]. Most relativistic dispersion calculations have been based on the Dory-Guest-Harris [*Dory et al.*, 1965] (DGH) distribution:

$$f(v_\parallel, v_\perp) = (\pi^{3/2}\alpha^3 l!)^{-1}(v_\perp^2/\alpha^2)^l \exp[-(v_\perp^2 + v_\parallel^2)/\alpha^2], \quad (2)$$

for which it is possible to derive analytic expressions for the dielectric elements in the semirelativistic approxi-

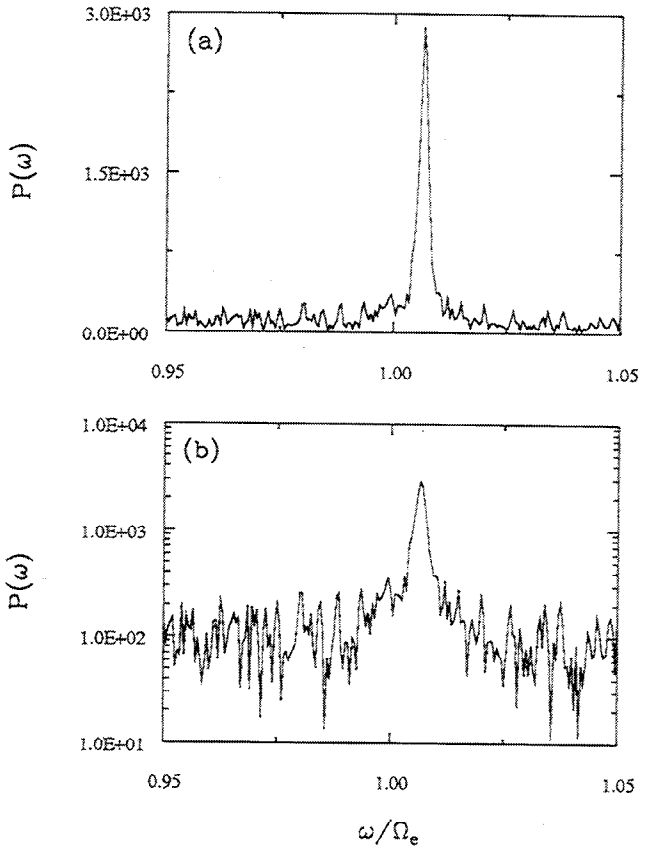

Figure 6. Same as Figure 5 but for the simulation using the 45° upgoing loss cone distribution.

mation [*Tsai et al.*, 1981; *Wu et al.*, 1981b; *Wong et al.*, 1982; *Winglee*, 1983; *Le Quéau et al.*, 1984a; *Yoon and Chang*, 1989]. In this procedure the relativistic gamma factor in the resonance denominator is approximated by $1+v^2/2c^2$, while all other relativistic corrections are neglected.

In (2), l is a positive integer and $\alpha = \sqrt{2}v_{Te} = (2T_e/m)^{1/2}$ is the thermal velocity. The maximum of (2) as a function of $v_\perp$ occurs for $v_{\perp 0}^2 = l\alpha^2$, and the halfwidth of the distribution is $\delta v_\perp/v_{\perp 0} = (4l)^{-1/2}$ for $l \gg 1$. Thus the DGH distribution has an enhancement at large pitch angles. While it clearly does not model in detail the type of horseshoe distribution indicated in Figure 1, we shall find that the growth rates and angular distribution are in very good agreement with the present simulation results. Thus the DGH distribution provides an adequate model for determining the bandwidth of the maser instability.

We use the DGH dielectric elements to solve for the (complex) wave frequency $\omega = \omega_r + i\gamma$ as a function of the (real) wavenumber k. This allows us to determine the maximum growth rate γ_m. Now consider the wave spectrum as a function of time. In the linear stage the field amplitude will vary as $E = E_0 e^{\gamma t}$ and the field intensity as $E^2 = E_0^2 e^{2\gamma t}$. After n e-foldings based on the maximum growth rate ($t = n/\gamma_m$), we have $E^2 = E_0^2 e^{2n\gamma/\gamma_m}$. We want to determine the frequency for which the spectrum is reduced to $1/e$ of its maximum value. This will occur for $2n\gamma_n/\gamma_m = 2n-1$ or $\gamma_n/\gamma_m = 1-1/2n$. If $n = 1$, for example, then $\gamma_1/\gamma_m = 1/2$, and we recover the full width at half maximum of the linear theory. For $n > 1$, $\gamma_n \to \gamma_m$, and the peak will sharpen.

The peak growth rate for the DGH distribution occurs for $k_\parallel = 0$. We have solved the R-X mode dispersion relation for $l = 2$ and $c^2/\alpha^2 = 100$ and 200 corresponding to peak energies of 5 and 2.5 keV, respectively. The corresponding thermal energies $mv_{Te}^2/2$ are 1.3 and 0.64 keV. The real frequency and growth rate at maximum growth for the case of $\Omega_e/\omega_{pe} = 50$ are $\omega_m/\Omega_e = 0.9942$ and $\gamma_m/\Omega_e = 0.00312$ for $c^2/\alpha^2 = 100$ and 0.9977 and 0.00262 for $c^2/\alpha^2 = 200$. Figure 7a shows the linear growth curve as a function of ω for the case of $c^2/\alpha^2 = 100$. Figure 7b shows an expanded version of the growth curve in the vicinity of maximum growth.

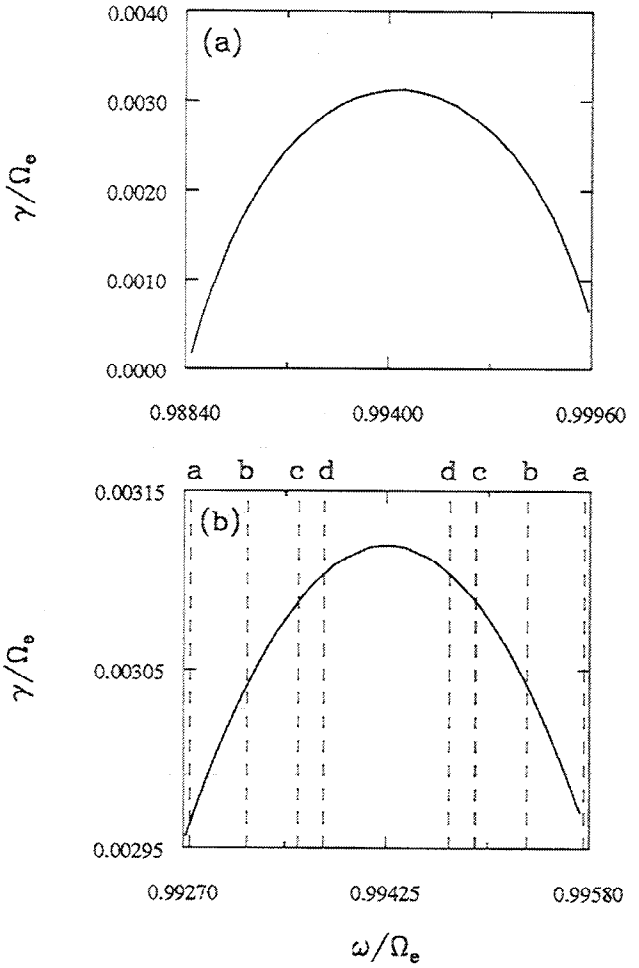

Figure 7. (a) Growth rate γ/Ω_e as a function of the frequency ω/Ω_e for the electron-cyclotron maser instability computed for the DGH distribution (2) using $c^2/\alpha^2 = 100$, $l = 2$, and $\Omega_e/\omega_{pe} = 50$. (b) A portion of the growth curve from a in the vicinity of maximum growth. The vertical dashed lines marked a, b, c, and d indicate the location of the $1/e$ power points that would be obtained after $n = 10$, 20, 50, and 100 e-foldings in amplitude, respectively.

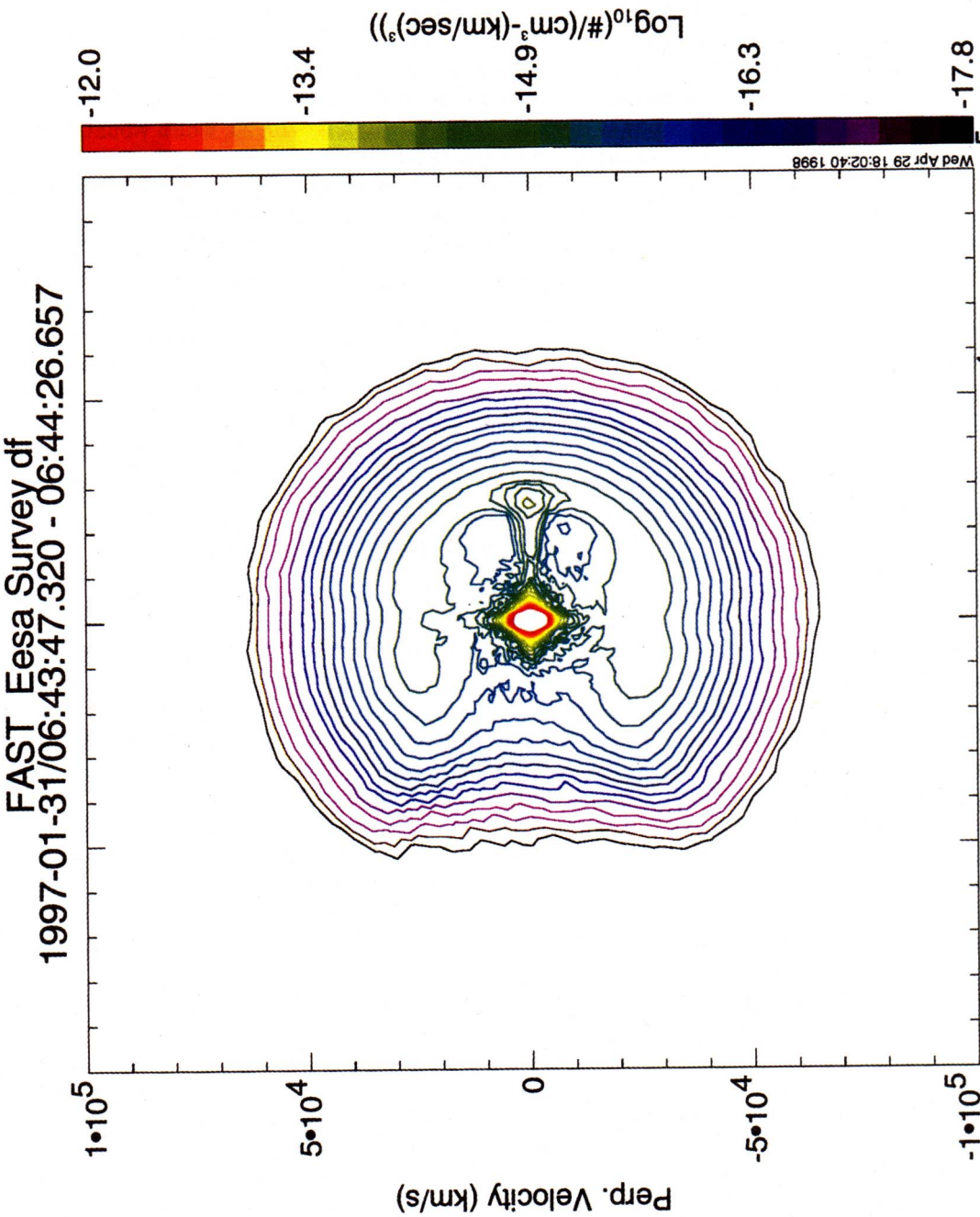

FIG. 1. Electron contour plots in $v_\perp, v_\parallel$ space from a FAST crossing of the AKR source region on orbit 1761.

The lines marked a indicate the $1/e$ power points after $n = 10$ e-foldings, while those marked b, c, and d correspond to $n = 20$, 50, and 100, respectively. Table 1 gives the numerical values of the bandwidths with $\Omega_e/\omega_{pe} = 50$ and $l = 2$ for various values of n for the cases of $c^2/\alpha^2 = 100$ and 200.

These results for the $1/e$ bandwidths are relatively insensitive to the parameter l in (2) which controls the thermal spread of the distribution relative to the peak. With $l\alpha^2$ held fixed, changing l from 2 to 8 for $n = 20$, for example, changes $\Delta\omega/\Omega_e$ from 0.00214 to 0.00159. As Ω_e/ω_{pe} is increased, the bandwidth $\Delta\omega$ decreases. For $l = 2$, $c^2/\alpha^2 = 100$, and $n = 10$, the variation is from 0.00404 to 0.00301 to 0.00247 as Ω_e/ω_{pe} changes from 20 to 50 to 100.

The results of the linear theory analysis are in very good agreement with the simulations. Thus, for $c^2/\alpha^2 = 100$, $\Omega_e/\omega_{pe} = 50$, and $l = 2$, the maximum growth rate is $\gamma_m/\Omega_e = 3.12 \times 10^{-3}$ as compared with 3.1×10^{-3} in the simulation. In the simulation saturation occurred after $n = 6.9$ e-foldings in the field amplitude. The corresponding bandwidth is $\Delta\omega/\Omega_e \approx 0.0037$, which agrees well with the observed value of 0.0030.

It has been estimated [*Omidi and Gurnett*, 1982] that an amplitude amplification of the order of e^{10} (i.e., $n = 10$, which corresponds to a power gain of e^{20} or 87 dB) above cosmic noise background levels is necessary to explain the observed level of AKR. Since the FAST observations [*Ergun et al.*, 1998] reveal much higher power levels of AKR in the source region, it is likely that this estimate should be increased to $n \approx 14$ (122 dB). From Table 1 we see that the corresponding bandwidth should be $\Delta\omega/\Omega_e \sim 0.002$. For a typical gyrofrequency of $f_{ce} \approx 440$ kHz in the source region sampled by FAST, this gives a bandwidth of the order of 1 kHz. To achieve a bandwidth as small as 100 Hz would require of the order of 500–1000 e-foldings.

To estimate the power level that could be produced by the maser instability in the auroral plasma cavity, we need to compare the convective growth length L_c with the transverse size of the cavity. L_c is given by $L_c = v_g/\gamma$, where v_g is the group velocity. Thus $L_c/\lambda = (2\pi)^{-1}(v_g/c)(\Omega_e/\gamma)(kc/\Omega_e)$, where λ is the wavelength of the radiation. The value of v_g/c is rather sensitive to the energy and the values of Ω_e/ω_{pe} and l. For $c^2/\alpha^2 = 100$, $l = 2$, and $\Omega_e/\omega_{pe} = 50$, $v_g/c = 0.46$ and $L_c/\lambda = 23$. If c^2/α^2 is increased to 200, then $v_g/c = 0.28$ and $L_c/\lambda = 16$. If c^2/α^2 and l are increased to 800 and 8, respectively, then $v_g/c = 0.29$ and $L_c/\lambda = 9.1$. In a less depleted cavity with $\Omega_e/\omega_{pe} = 20$ where the value of γ/Ω_e increases to 5.9×10^{-3}, then for $c^2/\alpha^2 = 100$ and $l = 2$, L_c/λ is only 5.5. On the other hand, if Ω_e/ω_{pe} is as large as 100, then γ/Ω_e drops to 1.4×10^{-3}, and L_c/λ rises to 76 for $l = 2$ and $c^2/\alpha^2 = 100$. Thus a reasonable range for L_c/λ is ~10–25, which would correspond to a length of 6.8–17 km for a wavelength of 0.68 km. Fourteen e-foldings would then require a pathlength of 95–240 km. The density-depleted cavities observed by FAST ranged from 30 to 300 km in latitudinal width. Thus it is reasonable to conclude that the spectral levels observed by FAST could be produced by the maser instability driven by the primary auroral electron distribution without any additional effect such as feedback. On the other hand, it would clearly not be possible to achieve the extreme level of 500–1000 e-foldings in a single transit of the auroral cavity that would be needed to produce a bandwidth as small as 100 Hz.

Table 1. Frequency Bandwidth for Various Number n of e-Foldings

	$\Delta\omega/\Omega_e$	
n	$c^2/\alpha^2 = 100$	$c^2/\alpha^2 = 200$
1	0.00884	0.00537
5	0.00420	0.00287
10	0.00301	0.00189
20	0.00214	0.00134
50	0.00136	0.00085
100	0.00096	0.00060

5. Summary and Discussion

The FAST mission has obtained wave and electron observations in the AKR source region with greatly improved frequency and time resolution as compared to previous measurements. Despite this unprecedented resolution, the electron particle distributions are dominated by a large plateau covering pitch angles from near field-aligned all the way to the loss cone. This suggests that the distributions have been rapidly stabilized by AKR wave growth on an even faster timescale. Further, the source region has been confirmed to be dominated by hot electrons and is nearly void of low-energy electrons. The ratio of the electron cyclotron frequency to plasma frequency Ω_e/ω_{pe} is then on the order of 50 or higher.

The nature of these diffused electron distributions has been investigated by means of 2-D, initial value, relativistic, electromagnetic particle simulations. The initial electron distribution was constructed by integrating the FAST electron distribution over $v_\perp$ and assuming that the reduced distribution should be consistent with the accessibility boundary for electrons of magnetospheric origin; this results in a "horseshoe" shaped distribution. Such a distribution is ideally suited to satisfy the cyclotron resonance condition with wave emission perpendicular to the ambient magnetic field ($k_\parallel = 0$), and the resulting cyclotron maser emissions are found to produce a strong diffusion of the electrons to lower values of $v_\perp$ on timescales of the order of 5000 Ω_e^{-1} (a few milliseconds). The free energy in the primary electron distribution is sufficient to produce electric fields

on the order of 500 mV/m, consistent with the FAST observations. The plateaued distributions observed by FAST are thus seen to be consistent with a process in which the increase of the perpendicular velocity of the electrons as they propagate into a region of increasing magnetic field strength is balanced by the diffusion to lower $v_\perp$ caused by the maser instability.

While the upgoing loss cone does contribute to some extent in driving the maser instability in the present simulations, the results are quite different from the case of the pure loss cone driven instability originally envisioned by *Wu and Lee* [1979]. In order to satisfy the resonance condition for such a distribution, a finite value of $k_\parallel$ is required, corresponding to emission at a substantial angle ($\gtrsim 10°$) away from perpendicular to the magnetic field. The FAST observations reveal that the wave propagation in the source region is consistent with $k_\parallel = 0$ to within a few degrees. Also, the pure loss cone distribution produces wave emission at frequencies above Ω_e and would thus not be able to explain the observations extending below Ω_e down to the relativistic cyclotron frequency. Simulations for the idealized case of a perfectly sharp 45° loss cone indicate that the maser field energy is considerably weaker than is produced by the horseshoe type distribution. Finally, the diffusion produced by the loss cone driven instability affects only the upgoing electrons and thus cannot produce the broad plateau covering the downgoing electrons which is characteristic of the FAST observations.

In the present simulations, which were carried out in a strictly uniform geometry, saturation occurred after some 7 e-foldings in the field amplitude, and the observed full width at the $1/e$ power points was $\Delta\omega/\Omega_e \approx 0.003$. Linear theory estimates show that for the more realistic case of ~14 e-foldings above the cosmic noise background levels, this bandwidth would be reduced only to $\Delta\omega/\Omega_e \approx 0.002$. Thus the intrinsic maser bandwidth in a uniform geometry with parameters characteristic of the AKR source region is ~ 0.5–1.0 kHz. This is indeed comparable to some of the observed AKR fine structure, but it is considerably broader than the finest structures (100 Hz and below) which have been reported. It is apparently not possible to produce 100 Hz structures from a single transit of maser radiation across the observed few hundred km wide auroral cavity.

The present simulations suffer from the limitations of the initial value approach and the assumption of a uniform magnetic field and plasma configuration. A much more realistic approach would be to incorporate the FAST particle distributions into a driven model of the AKR source region such as that considered by *Pritchett and Winglee* [1989]. The results of this model (in a very limited spatial domain with dimensions of tens of kilometers) indicated that the AKR maser radiation should possess a multiple wavepacket structure with individual bursts occurring on millisecond timescales. These results are intriguingly similar to the bursty nature of the FAST observations in the AKR source region reported by *Strangeway et al.* [1998b], and this similarity suggests the obvious next step for a comparison of simulations and observations.

Acknowledgments. The research of PLP was supported by NASA grant NAG 5-3235, and the research of the FAST members was supported by NASA grant NAG 5-3596.

Hiroshi Matsumoto thanks A. Roux and another referee for their assistance in evaluating this paper.

References

Baumback, M. M., and W. Calvert, The minimum bandwidths of auroral kilometric radiation, *Geophys. Res. Lett., 14*, 119, 1987.

Benediktov, E. A., G. G. Getmantsev, Y. A. Sazonov, and A. F. Tarasov, Preliminary results of measurements of the intensity of distributed extraterrestrial radio frequency emission at 725 and 1525 kHz frequency by the satellite Electron-2, *Kosm. Issled., 3*, 614, 1965. [*Cosmic Res.*, Engl. Trans., *3*, 492, 1968].

Calvert, W., A feedback model for the source of auroral kilometric radiation, *J. Geophys. Res., 87*, 8199, 1982.

Calvert, W., An explanation for auroral structure and the triggering of auroral kilometric radiation, *J. Geophys. Res., 100*, 14,887, 1995.

Chiu, Y. T., and M. Schulz, Self-consistent particle and parallel electrostatic field distributions in the magnetospheric-ionospheric auroral region, *J. Geophys. Res., 83*, 629, 1978.

de Feraudy, H., B. M. Pedersen, A. Bahnsen, and M. Jespersen, Viking observations of auroral kilometric radiation from the plasmasphere to night auroral oval source regions, *Geophys. Res. Lett., 14*, 511, 1987.

Delory, G. T., R. E. Ergun, C. W. Carlson, L. Muschetti, C. C. Chaston. W. Peria, J. P. McFadden, and R. Strangeway, FAST observations of electron distributions within AKR source regions, *Geophys. Res. Lett., 25*, 2069, 1998.

Dory, R. A., G. E. Guest, and E. G. Harris, Unstable electrostatic plasma waves propagating perpendicular to a magnetic field, *Phys. Rev. Lett., 14*, 131, 1965.

Ergun, R. E., et al., FAST satellite wave observations in the AKR source region, *Geophys. Res. Lett., 25*, 2061, 1998.

Gurnett, D. A., The Earth as a radio source: Terrestrial kilometric radiation, *J. Geophys. Res., 79*, 4227, 1974.

Gurnett, D. A., and R. R. Anderson, The kilometric radio emission spectrum: Relation to auroral acceleration processes, in *Physics of Auroral Arc Formation, Geophys. Monogr. Ser.*, vol. 25, edited by S.-I. Akasofu and J. R. Kan, p. 341, AGU, Washington, D. C., 1981.

Gurnett, D. A., R. R. Anderson, F. L. Scarf, R. W. Fredricks, and E. J. Smith, Initial results from the ISEE 1 and 2 plasma wave investigation, *Space Sci. Rev., 23*, 103, 1979.

Gurnett, D. A., S. D. Shawhan, and R. R. Shaw, Auroral hiss, Z mode radiation, and auroral kilometric radiation in the polar magnetosphere: DE 1 observations, *J. Geophys. Res., 88*, 329, 1983.

Kurth, W. S., M. M. Baumback, and D. A. Gurnett, Direction-finding measurements of auroral kilometric radiation, *J. Geophys. Res., 80*, 2764, 1975.

Le Quéau, D., R. Pellat, and A. Roux, Direct generation of the auroral kilometric radiation by the maser synchrotron instability: An analytical approach, *Phys. Fluids, 27*, 247, 1984a.

Le Quéau, D., R. Pellat, and A. Roux, Direct generation of the auroral kilometric radiation by the maser synchrotron

instability: Physical mechanism and parametric study, *J. Geophys. Res., 89*, 2831, 1984b.

Le Quéau, D., R. Pellat, and A. Roux, The maser synchrotron instability in an inhomogeneous medium: Application to the generation of the auroral kilometric radiation, *Ann. Geophys., 3*, 273, 1985.

Louarn, P., A. Roux, H. de Féraudy, D. Le Quéau, M. André, and L. Matson, Trapped electrons as a free energy source for the auroral kilometric radiation, *J. Geophys. Res., 95*, 5983, 1990.

Menietti, J. D., J. L. Burch, R. M. Winglee, and D. A. Gurnett, DE 1 particle and wave observations in auroral kilometric radiation (AKR) source regions, *J. Geophys. Res., 98*, 5865, 1993.

Omidi, N., and D. A. Gurnett, Growth rate calculations of auroral kilometric radiation using the relativistic resonance condition, *J. Geophys. Res., 87*, 2377, 1982.

Pritchett, P. L., Relativistic dispersion, the cyclotron maser instability, and auroral kilometric radiation, *J. Geophys. Res., 89*, 8957, 1984.

Pritchett, P. L., The electron-cyclotron maser instability in relativistic plasmas, *Phys. Fluids, 29*, 2919, 1986a.

Pritchett, P. L., Cyclotron maser radiation from a source structure localized perpendicular to the ambient magnetic field, *J. Geophys. Res., 91*, 13,569, 1986b.

Pritchett, P. L., and R. J. Strangeway, A simulation study of kilometric radiation generation along an auroral field line, *J. Geophys. Res., 90*, 9650, 1985.

Pritchett, P. L., and R. M. Winglee, Generation and propagation of kilometric radiation in the auroral plasma cavity, *J. Geophys. Res., 94*, 129, 1989.

Roux, A., A. Hilgers, H. de Feraudy, D. Le Queau, P. Louarn, S. Perraut, A. Bahnsen, M. Jespersen, E. Ungstrup, and M. Andre, Auroral kilometric radiation sources: In situ and remote observations from Viking, *J. Geophys. Res., 98*, 11,657, 1993.

Strangeway, R. J., Wave dispersion and ray propagation in a weakly relativistic electron plasma: Implications for the generation of auroral kilometric radiation, *J. Geophys. Res., 90*, 9675, 1985.

Strangeway, R. J., et al., FAST observations of VLF waves in the auroral zone: Evidence of very low plasma densities, *Geophys. Res. Lett., 25*, 2065, 1998a.

Strangeway, R. J., P. L. Pritchett, R. E. Ergun, C. W. Carlson, J. P. McFadden, G. T. Delory, and R. C. Elphic, Observations by FAST of fine-scale frequency structure in auroral kilometric radiation, *Eos, Trans. AGU, 79*(17), Spring Meet. Suppl., S308, 1998b.

Tsai, S. T., C. S. Wu, Y. D. Wang, and S. W. Kang, Dielectric tensor of a weakly relativistic, nonequilibrium, and magnetized plasma, *Phys. Fluids, 24*, 2186, 1981.

Ungstrup, E., A. Bahnsen, H. K. Wong, M. André, and L. Matson, Energy source and generation mechanism for auroral kilometric radiation, *J. Geophys. Res., 95*, 5973, 1990.

Winglee, R. M., Interrelation between azimuthal bunching and semi-relativistic maser cyclotron instabilities, *Plasma Phys., 25*, 217, 1983.

Winglee, R. M., and P. L. Pritchett, The generation of low-frequency electrostatic waves in association with auroral kilometric radiation, *J. Geophys. Res., 91*, 13,531, 1986.

Wong, H. K., C. S. Wu, F. J. Ke, R. S. Schneider, and L. F. Ziebell, Electromagnetic cyclotron-loss-cone instability associated with weakly relativistic electrons, *J. Plasma Phys., 28*, 503, 1982.

Wu, C. S., and L. C. Lee, A theory of the terrestrial kilometric radiation, *Astrophys. J., 230*, 621, 1979.

Wu, C. S., S. T. Tasi, M. J. Xu, and J. W. Shen, Saturation and energy-conversion efficiency of auroral kilometric radiation, *Astrophys. J., 248*, 384, 1981a.

Wu, C. S., C. S. Lin, H. K. Wong, S. T. Tsai, and R. L. Zhou, Absorption and emission of extraordinary-mode electromagnetic waves near cyclotron frequency in nonequilibrium plasmas, *Phys. Fluids, 24*, 2191, 1981b.

Yoon, P. H., and T. Chang, Exact dielectric tensor for relativistic magnetized plasma with loss-cone and field-aligned drift, *J. Plasma Phys., 42*, 193, 1989.

C. W. Carlson, G. T. Delory, R. E. Ergun, and J. P. McFadden, Space Sciences Laboratory, University of California, Berkeley, CA 94720-7450.

P. L. Pritchett, Department of Physics and Astronomy, University of California, 405 Hilgard Avenue, Los Angeles, CA 90095-1547. (pritchet@physics.ucla.edu)

R. J. Strangeway, Institute of Geophysics and Planetary Physics, University of California, 405 Hilgard Avenue, Los Angeles, CA 90095-1567. (strange@igpp.ucla.edu)

(Received August 25, 1998; revised December 15, 1998; accepted December 15, 1998.)